phys. stat. sol. (b) 119, 595 (1983)

Subject classification: 14.3 and 20.1; 6; 13.5.2; 22.2.2

Sektion Physik der Bergakademie Freiberg<sup>1</sup>) (a) and A. F. Ioffe Physico-Technical Institute, Academy of Sciences of the USSR, Leningrad (b)

# Determination of the Charge Carrier Concentration and Mobility in n-GaP by Raman Spectroscopy

 $\mathbf{B}\mathbf{y}$ 

G. IRMER (a), V. V. TOPOROV (b), B. H. BAIRAMOV (b), and J. MONECKE (a)

A method is presented which allows the determination of the charge carrier concentration and mobility in n-GaP by Raman spectroscopy of coupled plasmon-phonon modes. The results are compared with those of electrical measurements.

Es wird eine Methode für die Bestimmung der Konzentration freier Ladungsträger und deren Beweglichkeit in n-GaP mittels Raman-spektroskopischer Messungen gekoppelter Plasmon-Phonon-Moden vorgestellt. Die Ergebnisse werden mit denen elektrischer Messungen verglichen.

#### 1. Introduction

In a polar semiconductor the free carrier plasma interacts with the longitudinal-optical lattice vibrations (LO-phonons) via their macroscopic electric fields. As a result of this interaction instead of a pure plasmon and a pure LO-phonon two coupled modes appear which have mixed plasmon-phonon character. A method to measure the frequencies, bandwidths, and intensities of these coupled modes is provided by Raman scattering and yields information about the concentration and the mobility of the free carriers. Coupled plasmon-phonon modes were first proposed by Varga [1] and first observed by Mooradian and Wright [2] in GaAs and by Hon and Faust [3] in GaP.

In this paper we give a discussion of the influence of phonon damping on the Raman scattering efficiency of plasmon-phonon modes in GaP and propose an easy procedure in order to determine the concentration and the mobility of free carriers from the frequency and the bandwidth of the higher-frequency coupled mode.

The optical determination of electrical parameters has some advantages: It is not necessary to contact the sample and the local resolution is high in comparison with electrical measurements and limited by the possibility of focusing laser beams only.

We performed Raman measurements on many differently doped samples of GaP and compared the values of the carrier concentrations and the mobilities with the results of conductivity and Hall-effect measurements. The data obtained are in good agreement.

## 2. Theory of Raman Scattering from Coupled Plasmon-Phonon Modes

Raman scattering from coupled plasmon-LO-phonon modes occurs by means of the following mechanisms:

A) modulation of the optical polarizability by the atomic displacements (deforma-

<sup>1)</sup> B. v. Cotta-Str. 4, DDR-9200 Freiberg, GDR.

tion potential scattering) and by the macroscopic longitudinal electric field (electrooptical scattering),

B) scattering due to density fluctuations of the free carriers.

The Raman efficiencies due to these mechanisms where deduced by several authors [4 to 6]. We follow the derivation given by Klein et al. [5] which is correct also in the case of large plasmon damping [6], and we take into consideration phonon damping additionally.

The Raman efficiencies due to the mechanisms A) and B) are given by [5] and can be converted into the form

A) 
$$I_{A} = \frac{\mathrm{d}^{2}R}{\mathrm{d}\omega \,\mathrm{d}\Omega}\Big|_{A} = \frac{16\pi\hbar n_{2}}{V_{0}^{2}n_{1}} \left(\frac{\omega_{2}}{c}\right)^{4} \left(\frac{\partial\alpha}{\partial E^{L}}\right)^{2} (n_{\omega} + 1) A \,\mathrm{Im}\left(-\frac{1}{\varepsilon}\right),$$
 (1)

where

$$A = \left[ \frac{\omega_{\mathrm{T}}^2 (1+C) - \omega^2}{\omega_{\mathrm{T}}^2 - \omega^2} \right]^2 \tag{2}$$

with

$$C = \frac{e^*}{\omega_T^2 M} \left( \frac{(\partial \alpha / \partial u)}{(\partial \alpha / \partial E^{\perp})} \right) \tag{3}$$

being the so-called "Faust-Henry coefficient" [7], which determines the ratio of scattering by LO- and TO-phonons in an undoped crystal,

$$\frac{(\mathrm{d}^2 R/\mathrm{d}\omega \,\mathrm{d}\Omega)|_{\mathrm{LO}}}{(\mathrm{d}^2 R/\mathrm{d}\omega \,\mathrm{d}\Omega)|_{\mathrm{TO}}} = \left(\frac{\omega_1 + \omega_L}{\omega_1 + \omega_T}\right)^4 \frac{\omega_T}{\omega_L} \left(1 + \frac{\omega_T^2 - \omega_L^2}{C\omega_T^2}\right)^2,\tag{4}$$

and with

$$\frac{\partial \alpha}{\partial u} = \sum_{i,j,k} e_{0i} e_{1j} e_{2k} \frac{\partial \alpha_{jk}}{\partial u_i},\tag{5}$$

$$\frac{\partial \alpha}{\partial E^{L}} = \sum_{i,j,k} e_{0i} e_{1j} e_{2k} \frac{\partial \alpha_{jk}}{\partial E_{i}^{L}}.$$
 (6)

The following notations are used:  $\omega_{1/2}$  incident and scattered photon frequencies, respectively,  $n_{1/2}$  refractive indices of the crystal at  $\omega_{1/2}$ ,  $\omega = \omega_1 - \omega_2$  Raman frequency (energy transfer),  $\omega_{\text{L/T}}$  LO- and TO-phonon frequencies,  $V_0$  volume of the unit cell,  $e^*$  effective charge associated with the optical phonons; M reduced mass;  $n_\omega = [\exp{(\hbar\omega/k_BT)}-1]^{-1}$  Bose-Einstein factor,  $e_0$  unit vector parallel q,  $q = k_1 - k_2$  transfered wave vector,  $e_{1/2}$  incident and scattered photon polarization unit vectors, u displacement,  $E^{\text{L}}$  macroscopic electrical field,  $\alpha_{jk}$  polarizability.

B) 
$$I_{\rm B} = \frac{\mathrm{d}^2 R}{\mathrm{d}\omega \,\mathrm{d}\Omega}\Big|_{\rm B} = \frac{\hbar n_2}{\pi n_1} \left(\frac{\omega_2}{c}\right)^4 \left(\frac{eq\mu}{\omega_1\omega_2}\right)^2 (n_\omega + 1) \, B \,\mathrm{Im}\left(-\frac{1}{\varepsilon}\right),$$
 (7)

where

$$B = \left[\frac{\omega_{\rm L}^2 - \omega^2}{\omega_{\rm T}^2 - \omega^2}\right]^2 \tag{8}$$

and

$$\mu = \sum_{i \mid k} e_{1j} e_{2k} \mu_{jk} \tag{9}$$

with  $\mu_{ik}$  being the reciprocal effective mass tensor.

Equations (1) and (7) were derived in [5] without taking into account phonon damping, which can be neglected in that case of heavily doped SiC. In our case of low doped GaP we have to take into consideration phonon damping, too. This alters the expressions of the Raman efficiencies given above in the following way: The dielectric function  $\varepsilon$  in the presence of free carriers is given by

$$\varepsilon = \varepsilon_{\infty} \left\{ 1 + \frac{\omega_{\rm L}^2 - \omega_{\rm T}^2}{\omega_{\rm T}^2 - \omega^2 - i\omega_{\rm Y}} - \frac{\omega_{\rm p}^2}{\omega(\omega + i\Gamma)} \right\},\tag{10}$$

where

$$\omega_{\rm p} = \sqrt{\frac{4\pi e^2 n}{\epsilon_{\infty} m^*}} \tag{11}$$

is the plasma frequency,  $\gamma$  the phonon damping constant, and n and  $m^*$  are the concentration and the effective mass of the free carriers, respectively.

As the effective mass  $m^*$  the bare mass and not the (experimentally measured) polaron mass has to be used. According to Beni and Rice [8] the values of the bare masses for electrons in GaP are  $m_{||} = 1.781 m_0$ ,  $m_{\perp} = 0.25 m_0$ . The effective mass then is given by

$$m^* = \left[\frac{1}{3}\left(\frac{2}{m_{\perp}} + \frac{1}{m_{||}}\right)\right]^{-1} = 0.3504m_0. \tag{12}$$

Due to the cubic symmetry  $m^*$  is independent of the direction of the q-vector: The directional dependence is cancelled out by averaging over all six sections of a line parallel to the q-vector with the six energy ellipsoids of the conduction band in the vicinity of the X-points.

Including phonon damping the functions A and B in (1) and (7) are given by

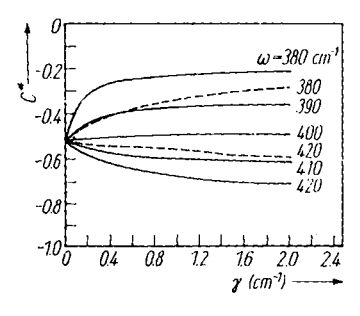
$$A = \frac{\left(\omega_{\rm T}^{2}(1 + C^{*}) - \omega^{2}\right)^{2}}{(\omega_{\rm T}^{2} - \omega^{2})^{2}} = 1 + 2C\omega_{\rm T}^{2} \frac{\omega_{\rm p}^{2}\Gamma(\omega_{\rm T}^{2} - \omega^{2}) - \omega^{2}\gamma(\omega^{2} + \Gamma^{2})}{\omega_{\rm p}^{2}\Gamma[(\omega_{\rm T}^{2} - \omega^{2})^{2} + \omega^{2}\gamma^{2}] + \omega^{2}\gamma(\omega_{\rm L}^{2} - \omega_{\rm T}^{2})(\omega^{2} + \Gamma^{2})} + C^{2} \frac{\omega_{\rm T}^{4}}{\omega_{\rm L}^{2} - \omega_{\rm T}^{2}} \frac{\omega_{\rm p}^{2}[\Gamma(\omega_{\rm L}^{2} - \omega_{\rm T}^{2}) + \gamma(\omega_{\rm p}^{2} - 2\omega^{2})] + \omega^{2}\gamma(\omega^{2} + \Gamma^{2})}{\omega_{\rm L}^{2} - \omega_{\rm T}^{2}} \frac{\omega_{\rm p}^{2}\Gamma[(\omega_{\rm T}^{2} - \omega^{2})^{2} + \omega^{2}\gamma^{2}] + \omega^{2}\gamma(\omega_{\rm L}^{2} - \omega_{\rm T}^{2})(\omega^{2} + \Gamma^{2})}{(\omega_{\rm T}^{2} - \omega^{2})^{2}} = \frac{(\omega_{\rm L}^{*2} - \omega^{2})^{2}}{(\omega_{\rm T}^{2} - \omega^{2})^{2}} = \frac{\omega_{\rm p}^{2}\Gamma(\omega_{\rm L}^{2} - \omega^{2})^{2} + \omega_{\rm p}^{4}\gamma(\omega_{\rm L}^{2} - \omega_{\rm T}^{2}) + \Gamma\gamma^{2}\omega_{\rm p}^{2}\omega^{2}}{\omega_{\rm p}^{2}\Gamma[(\omega_{\rm T}^{2} - \omega^{2})^{2} + \omega^{2}\gamma^{2}] + \omega^{2}\gamma(\omega_{\rm L}^{2} - \omega_{\rm T}^{2})(\omega^{2} + \Gamma^{2})}$$
(14)

instead of (2) and (8) (see Appendix). For  $\gamma = 0$  we obtain  $C^* = C$  and (13) reduces to (2) as given by Klein et al. [5].

The scattering according to the mechanism A) in the approximation (2) vanishes at  $\omega^2 = \omega_{\rm T}^2(1+C)$ . This allows, in principle, the experimental determination of the coefficient C and the ratio  $(\partial \alpha/\partial u)/(\partial \alpha/\partial E^{\rm L})$  (see [5, 9]).

In the case of  $\gamma \neq 0$  it must be taken into account that  $C^*$  is not a constant but a function of  $\omega$ . This function

$$C^* = \frac{\omega_{\mathrm{T}}^2 - \omega^2}{\omega_{\mathrm{T}}^2} \left( \sqrt{A} - 1 \right) \tag{15}$$



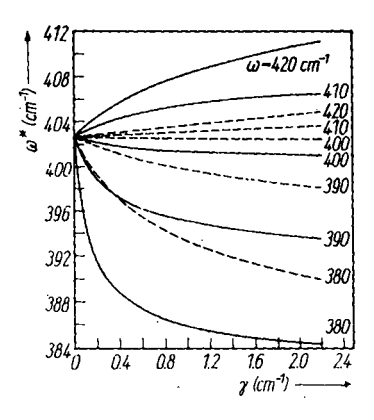


Fig. 1

Fig. 2

Fig. 1.  $C^*$  (equation (15)) as a function of phonon damping  $\gamma$  and frequency  $\omega$  for two different carrier concentrations and mobilities.  $---\omega_p=121.5~\mathrm{cm}^{-1}$  and  $\Gamma=359~\mathrm{cm}^{-1}$ ; ——— $\omega_p=45.3~\mathrm{cm}^{-1}$ ,  $\Gamma=276~\mathrm{cm}^{-1}$ 

Fig. 2.  $\omega^*$  (equation (16)) as a function of phonon damping  $\gamma$  and frequency  $\omega$  for two different carrier concentrations and mobilities.  $---\omega_p=121.5~\mathrm{cm}^{-1}$  and  $\Gamma=359~\mathrm{cm}^{-1}$ ;  $----\omega_p=45.3~\mathrm{cm}^{-1}$ ,  $\Gamma=276~\mathrm{cm}^{-1}$ 

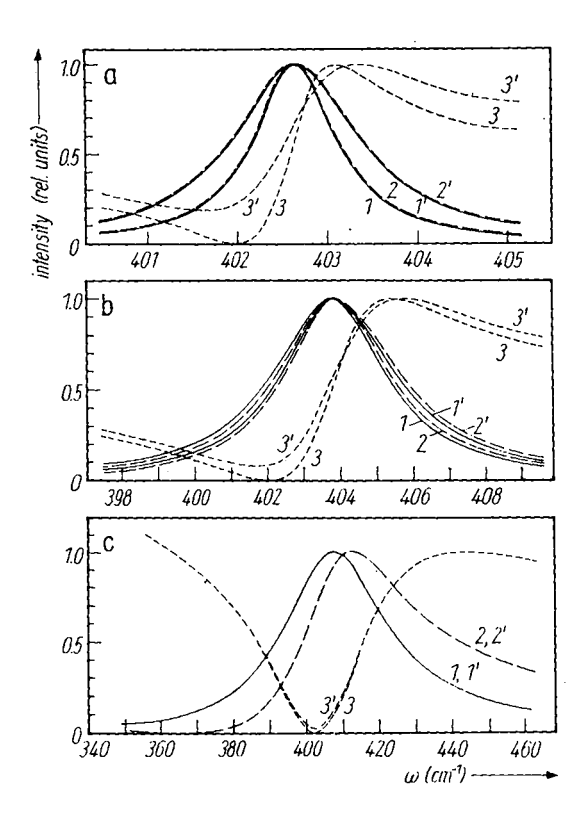


Fig. 3. Raman scattering intensity in the region of the upper mode  $\omega_+$  (theoretical profiles, normalized). a)  $\omega_p =$  = 70 cm<sup>-1</sup> and  $\Gamma = 326$  cm<sup>-1</sup>; b)  $\omega_p =$  = 122 cm<sup>-1</sup> and  $\Gamma = 359$  cm<sup>-1</sup>; c)  $\omega_p =$  = 362 cm<sup>-1</sup> and  $\Gamma = 677$  cm<sup>-1</sup>. (1)  $I_A$  (equation (1)) with A (equation (13)),  $\gamma = 0$  cm<sup>-1</sup>; (1)  $I_A$  (equation (13)),  $\gamma = 0.6$  cm<sup>-1</sup>; (2) Im (-1/ $\varepsilon$ ),  $\gamma = 0.6$  cm<sup>-1</sup>; (3)  $I_B$  (equation (7)) with B (equation (14)),  $\gamma = 0$  cm<sup>-1</sup>; (3')  $I_B$  (equation (7)) with B (equation (14)), C = 0.6 cm<sup>-1</sup>

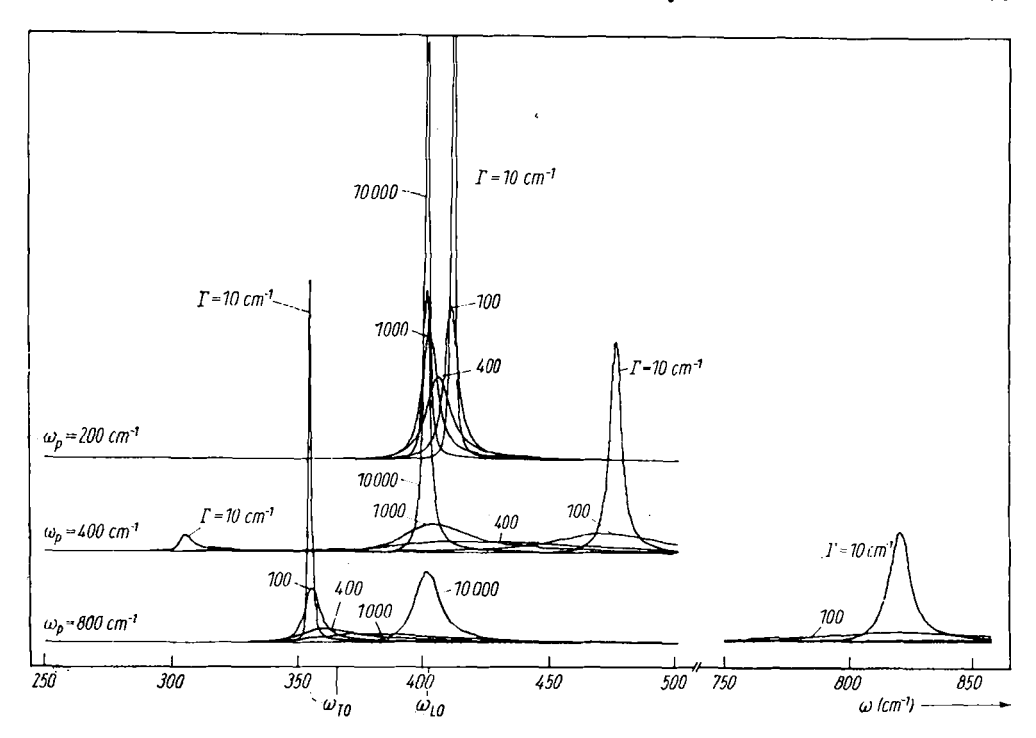


Fig. 4. Raman scattering efficiency  $I_{\rm A}$  (theoretical profiles) ( $\gamma=0.6~{
m cm^{-1}}$ )

is shown in Fig. 1 for different  $\omega$  and  $\gamma$ . The curves yield the Faust-Henry coefficient C=-0.53 of GaP for  $\gamma=0$ .

Fig. 2 illustrates the behaviour of the function

$$\omega^* = [(\omega_T^2 - \omega^2)\sqrt{B} + \omega^2]^{1/2}$$
 (16)

determining the scattering mechanism B). For  $\gamma = 0$ ,  $\omega^*$  reaches the value  $\omega^* = \omega_L$  derived in [5].

Fig. 3 demonstrates the influence of phonon damping on the lineshape for different frequencies and damping constants of the plasmons in the frequency region of the upper coupled mode. Whereas at low plasmon frequencies the inclusion of phonon damping is important, its influence can be neglected at higher plasmon frequencies.

Sometimes the simple expression  $I \sim \text{Im} (-1/\varepsilon)$  is used to describe the coupled-mode lineshape. For low plasmon frequencies the difference between  $\text{Im} (-1/\varepsilon)$  and the correct Raman efficiency is small as shown in Fig. 3a. However, for large  $\omega_p$  the complete expression  $I_A \sim A \text{ Im} (-1/\varepsilon)$  must be used (Fig. 3b, c).

The light scattering efficiency due to carrier density fluctuations has no zero near  $\omega_L$  as in the case of  $\gamma=0$ , if we take phonon damping into account. The relative minima (and maxima) in this region are frequency shifted compared with the undamped case. These aspects are not important for GaP, because the scattering mechanism A) dominates [6].

Fig. 4 shows the coupled plasmon-phonon modes, calculated according to (1) with A given by (13), for three plasma frequencies  $\omega_{\rm p} < \omega_{\rm L}$ ,  $\omega_{\rm p} \approx \omega_{\rm L}$ ,  $\omega_{\rm p} > \omega_{\rm L}$  and different damping constants. For low  $\omega_{\rm p}$  the lower mode with frequency  $\omega_{\rm p}$  practically disappears. For  $\omega_{\rm p} \approx \omega_{\rm L}$  the mode  $\omega_{\rm p}$  appears (in the case of plasmon damping

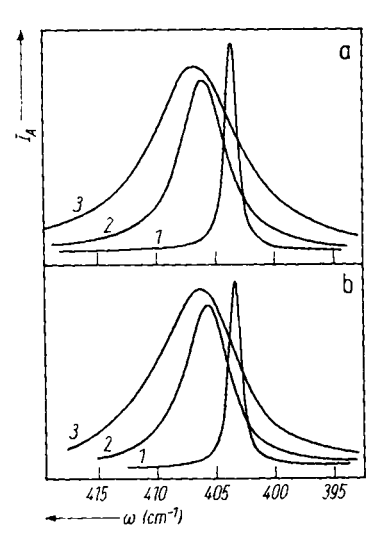


Fig. 5. Comparison of theoretical and experimental band shapes for differently doped n-GaP samples. (1)  $n=1.3\times10^{17}\,\mathrm{cm^{-3}}$ ,  $\mu=115\,\mathrm{cm^2\,V^{-1}\,s^{-1}}$ ; (2)  $6.0\times10^{17}$ , 95; (3)  $1.2\times10^{18}$ , 65. a)  $I_{\rm A}$ , calculated, b)  $I_{\rm A}$ , Raman measurement

 $\Gamma < 10 \text{ cm}^{-1}$ ) and dominates over the mode  $\omega_{+}$  in the range  $\omega_{p} > \omega_{L}$ . Increasing  $\omega_{p}$  the frequency  $\omega_{-}$  approaches  $\omega_{T}$  from the left (in the case of low plasmon damping compared with  $\omega_{p}$ ). In the range  $\omega_{p} > \omega_{L}$  for  $\Gamma \gg \omega_{p} \omega_{-}$  approaches  $\omega_{L}$ , the damping of the coupled mode is decreased down to the phonon damping.

An increased plasmon damping shifts the coupled mode  $\omega_+$  towards  $\omega_L$ . Its damping is determined by the plasmon damping. For  $\Gamma \gg \omega_p$ , however, the plasmon damping is not transferred to the coupled mode, the halfwidth of which approaches that of the phonon. The limited possibilities to dope GaP, however, restrict the range of realizable parameters ( $\mu \approx 10^2 \, \mathrm{cm}^2 \, \mathrm{V}^{-1} \, \mathrm{s}^{-1}$ ,  $n < 10^{19} \, \mathrm{cm}^{-3}$ ,  $\Gamma \approx 250 \, \mathrm{cm}^{-1}$ ,  $\omega_p < 650 \, \mathrm{cm}^{-1}$ ).

parameters ( $\mu \approx 10^2$  cm<sup>2</sup> V<sup>-1</sup> s<sup>-1</sup>,  $n < 10^{19}$  cm<sup>-3</sup>,  $\Gamma \approx 250$  cm<sup>-1</sup>,  $\omega_p < 650$  cm<sup>-1</sup>). The coupled mode  $\omega_-$  cannot be observed in practice because of its low intensity. Our analysis, therefore, concentrates on a small range of frequencies above  $\omega_L$ .

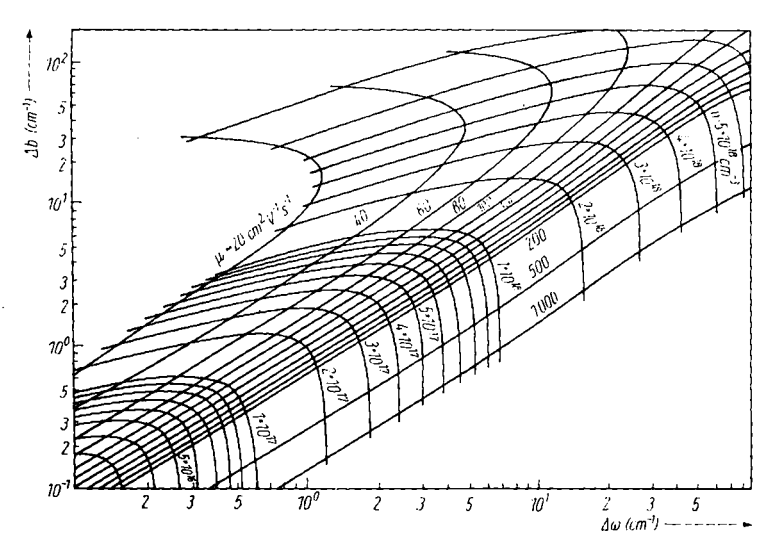


Fig. 6. Frequency and halfwidth shifts of the Raman mode  $\omega_+$  in dependence on the concentrations and mobilities of free carriers

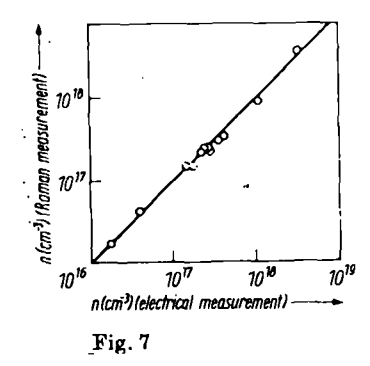
In order to obtain from the measured values  $\Delta\omega$  and  $\Delta b$  the electrical parameters n and  $\mu$  in an easy way we have calculated coupled modes  $\omega_+$  as functions of the frequency for many values of  $\omega_p$  and  $\Gamma$  using (1) with  $\Lambda$  from (13) and  $\varepsilon$  from (10). A computer program was employed to search for the maxima and halfwidths of the coupled modes  $\omega_+$ , the frequency shifts  $\Delta\omega$  and halfwidth broadenings  $\Delta b$  in comparison with the pure LO-phonons were listed. Fig. 6 represents the resulting nomogram. In the range of most interest ( $n=5\times10^{16}$  to  $5\times10^{18}$  cm<sup>-3</sup>,  $\mu=40$  to 200 cm<sup>2</sup> V<sup>-1</sup> s<sup>-1</sup>) the dependence of n and  $\mu$  on  $\Delta\omega$  and  $\Delta b$  is unique.

## 3. Experimental Results and Discussion

The Raman measurements were performed on different doped GaP:Te and GaP:S monocrystalline samples (size  $\approx 3 \times 5 \times 0.5 \text{ mm}^3$ ). As exciting source we used a Kr<sup>+</sup> laser ( $\lambda = 568.2 \text{ nm}, 200 \text{ mW}$ ), the scattered light was analysed with a modified variant of the double monochromator GDM 1000 (1300 grooves/mm) from VEB Carl Zeiss Jena and photon counting. The spectral slit width was about 0.3 cm<sup>-1</sup>.

As an example Fig. 5 shows the experimental line profiles of the mode  $\omega_+$  for three differently doped samples and the calculated profiles for comparison. From the measured values  $\Delta\omega$  and  $\Delta b$  the concentrations and mobilities of the free carriers were determined using the nomogram of Fig. 6. The same samples were measured electrically (conductivity and Hall-effect measurements). In Fig. 7 and 8 electrically and spectroscopically measured values are compared. Especially for the concentration the agreement is very good.

In order to explain the relatively larger deviations between the spectroscopical and electrical values of the mobility it is necessary to regard influences on the phonon frequencies and halfwidths besides of those given by plasmon-phonon coupling. Because the latter vanish at low temperatures we have measured the temperature dependence of the frequencies  $\omega$  and halfwidths b of the coupled mode on differently doped samples as shown in Fig. 9. These high-resolution Raman measurements were performed using a Fabry-Perot interferometer coupled with a double grating monochromator. The method used was described in [10] and yields for high-ohmic GaP  $(\varphi \approx 10^{12} \Omega \text{cm})$  a halfwidth of LO( $\Gamma$ )-phonons of b ( $=\gamma$ ) = (0.25  $\pm$  0.01) cm<sup>-1</sup> at



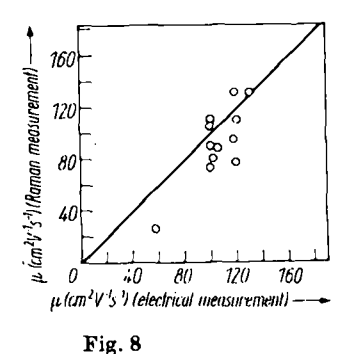


Fig. 7. Free-electron concentrations obtained by Raman measurements compared with results of electrical measurements

Fig. 8. Electron mobilities obtained by Raman measurements compared with results of electrical measurements

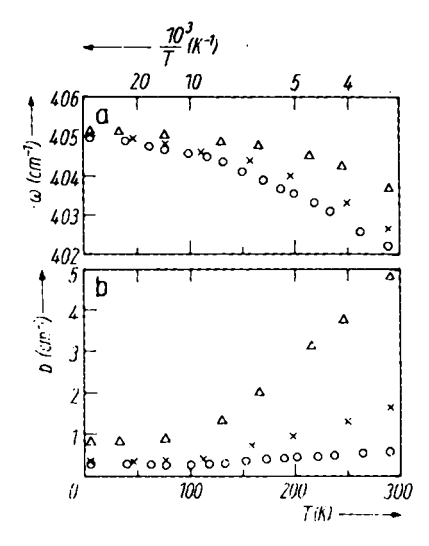


Fig. 9. Dependence of a) frequencies and b) halfwidths of the LO( $\Gamma$ )-phonons in insulating n-GaP (0  $\varrho \approx 10^{12} \Omega$  cm) and of the LO( $\Gamma$ )-phonon-plasmon modes of samples with different free-carrier concentrations (×  $n=1.6 \times 10^{17}$  cm<sup>-3</sup>;  $\Delta n=5.8 \times 10^{17}$  cm<sup>-3</sup>) on temperature

T extrapolated to 0 K and  $b=0.6~\rm cm^{-1}$  at room temperature.<sup>2</sup>) For higher impurity concentrations the halfwidth broadening does not vanish at low temperature. This residual influence of doping (besides of plasmon-phonon coupling) was not taken into account obtaining Fig. 7 and 8 and may be the reason for the deviations in the mobilities given in Fig. 8.

In a recent study of lifetimes of k=0 phonons in GaP with time delayed picosecond CARS [11] values of  $b=0.20~\rm cm^{-1}$  at  $T=5~\rm K$  and  $b=0.79~\rm cm^{-1}$  at room temperature were obtained. The deviation from our value at room temperature may be due to free carriers in the samples used in [11]. The reason for the deviation from our low-temperature value is not clear.

In summary, the method presented here yields excellent results for the determination of the free-carrier concentration and satisfactory results for the determination of their mobilities in n-GaP and is well suited in cases in which a high local resolution is demanded.

#### **Acknowledgements**

We would like to thank Dr. W. Siegel, Dr. E. Ziegler, and Dr. G. Kühnel for performing the electrical measurements.

## Appendix

According to [5] the phonon displacement and the electron density produce ionic and electronic contributions to the polarization  $P_q$  which has to be screened by the bound electron dielectric function  $\varepsilon_{\infty}$  (equation (2) of [5]).

The electric driving fields  $D_{i,e}$  acting on the ionic and electronic subsystems, are given by (4) and (5) in [5].

The Coulomb interaction within and between the subsystems is taken into consideration within the random-phase approximation. Linear response to the total

<sup>2)</sup> The latter value agrees with that obtained for high-ohmic samples with the double monochromator GDM 1000 and was used by us in order to obtain Fig. 7 and 8 from the nomogram of Fig. 6.

effective fields

$$D_{\rm i,e} = 4\pi \langle P_q \rangle / \varepsilon_{\infty}$$

induces the polarizations

$$\langle P_q^{\mathrm{i},\mathrm{e}} \rangle = \chi_{\mathrm{i},\mathrm{e}}(D_{\mathrm{l},\mathrm{e}} - 4\pi \langle P_q \rangle / \varepsilon_{\infty}) \; ,$$
 (A1)

where  $\chi_i$  and  $\chi_e$  are the susceptibilities for the ionic and free electronic systems, respectively. Instead of the  $\chi_i$  used in [5] (equation (8a)) we use

$$\chi_i = rac{\omega_{ extsf{L}}^2 - \omega_{ extsf{T}}^2}{\omega_{ extsf{T}}^2 - \omega^2 - i\omega\gamma}$$

taking phonon damping into account. Equation (A1) is then solved by

$$\langle P_q^j \rangle = \sum_{j'} \chi_{jj'} D_{j'}, \qquad (j, j' = i, e)$$
 (A2)

with

$$\chi_{jj'} = \chi_1 \delta_{jj'} - 4\pi \chi_1 \chi_{j'} / \varepsilon$$
.

 $\varepsilon$  is the dielectric function according to (10).

The calculated  $\chi_{jj'}$  are inserted into (16) of [5], giving the Raman efficiency with the factors A and B according to (13) and (14) instead of (2) and (8).

### References

- [1] B. B. Varga, Phys. Rev. 137, A1896 (1965).
- [2] A. MOORADIAN and G. B. WRIGHT, Phys. Rev. Letters 16, 999 (1966).
- [3] D. T. Hon and W. L. FAUST, Appl. Phys. 1, 241 (1973).
- [4] A. MOGRADIAN and L. Mc Whorter, in: Light Scattering Spectra of Solids, Ed. G. B. WRIGHT, Springer-Verlag, New York/Heidelberg/Berlin 1968.
- [5] M. V. KLEIN, B. N. GANGULY, and P. J. COLWELL, Phys. Rev. B 6, 2380 (1972).
- [6] M. V. Klein, in: Light Scattering in Solids, Ed. M. Cardona, Springer-Verlag, New York/ Heidelberg/Berlin 1975.
- [7] W. L. FAUST and C. R. HENRY, Phys. Rev. Letters 17, 1265 (1966).
- [8] G. BENI and T. M. RICE, Phys. Rev. B 18, 768 (1978).
- [9] J. F. Scott, T. C. Damen, and J. Shah, Optics Commun. 3, 384 (1971).
- [10] B. H. BAIRAMOV, D. A. PARSHIN, V. V. TOPOROV, and Sh. B. UBAIDULAEV, Zh. tekh. Fiz., Pisma 5, 1116 (1979).
- [11] J. Kuhl and W. E. Bron, Abstracts XVI. Internat. Conf. Phys. Semicond. Montpellier (France) 1982.

(Received April 25, 1983)